FIRST COSMOLOGY RESULTS USING TYPE IA SUPERNOVAE FROM THE DARK ENERGY SURVEY: CONSTRAINTS ON COSMOLOGICAL PARAMETERS

T. M. C. Abbott[1], S. Allam[2], P. Andersen[3,4], C. Angus[5], J. Asorey[6], A. Avelino[7], S. Avila[8], B. A. Bassett[9,10], K. Bechtol[11], G. M. Bernstein[12], E. Bertin[13,14], D. Brooks[15], D. Brout[12], P. Brown[16], D. L. Burke[17,18], J. Calcino[3], A. Carnero Rosell[19,20], D. Carollo[21], M. Carrasco Kind[22,23], J. Carretero[24], R. Casas[25,26], F. J. Castander[25,26], R. Cawthon[27], P. Challis[7], M. Childress[5], A. Clocchiatti[28], C. E. Cunha[17], C. B. D'Andrea[12], L. N. da Costa[20,29], C. Davis[17], T. M. Davis[3], J. De Vicente[19], D. L. DePoy[16], S. Desai[30], H. T. Diehl[2], P. Doel[15], A. Drlica-Wagner[2,31], T. F. Eifler[32,33], A. E. Evrard[34,35], E. Fernandez[24], A. V. Filippenko[36,37], D. A. Finley[2], B. Flaugher[2], R. J. Foley[38], P. Fosalba[25,26], J. Frieman[2,31], L. Galbany[39], J. García-Bellido[40], E. Gaztanaga[25,26], T. Giannantonio[41,42,43], K. Glazebrook[44], D. A. Goldstein[45], S. González-Gaitán[46], D. Gruen[17,18], R. A. Gruendl[22,23], J. Gschwend[20,29], R. R. Gupta[47], G. Gutierrez[2], W. G. Hartley[15,48], S. R. Hinton[3], D. L. Hollowood[38], K. Honscheid[49,50], J. K. Hoormann[3], B. Hoyle[51,43], D. J. James[52], T. Jeltema[38], M. W. G. Johnson[23], M. D. Johnson[23], E. Kasai[53,10], S. Kent[2,31], R. Kessler[54,31], A. G. Kim[47], R. P. Kirshner[55,56], E. Kovacs[57], E. Krause[32], R. Kron[2,31], K. Kuehn[58], S. Kuhlmann[57], N. Kuropatkin[2], O. Lahav[15], J. Lasker[54,31], G. F. Lewis[59], T. S. Li[2,31], C. Lidman[60], M. Lima[61,20], H. Lin[2], E. Macaulay[8], M. A. G. Maia[20,29], K. S. Mandel[62], M. March[12], J. Marriner[2], J. L. Marshall[16], P. Martini[49,63], F. Menanteau[22,23], C. J. Miller[34,35], R. Miquel[64,24], V. Miranda[32], J. J. Mohr[65,66,51], E. Morganson[23], D. Muthukrishna[67,41,60], A. Möller[67,60], E. Neilsen[2], R. C. Nichol[8], B. Nord[2], P. Nugent[47], R. L. C. Ogando[20,29], A. Palmese[2], Y.-C. Pan[68,69], A. A. Plazas[33], M. Pursiainen[5], A. K. Romer[70], A. Roodman[17,18], E. Rozo[71], E. S. Rykoff[17,18], M. Sako[12], E. Sanchez[19], V. Scarpine[2], R. Schindler[18], M. Schubnell[35], D. Scolnic[31], S. Serrano[25,26], I. Sevilla-Noarbe[19], R. Sharp[60], M. Smith[5], M. Soares-Santos[72], F. Sobreira[73,20], N. E. Sommer[67,60], H. Spinka[57], E. Suchyta[74], M. Sullivan[5], E. Swann[8], G. Tarle[35], D. Thomas[8], R. C. Thomas[47], M. A. Troxel[49,50], B. E. Tucker[67,60], S. A. Uddin[75], A. R. Walker[1], W. Wester[2], P. Wiseman[5], R. C. Wolf[76], B. Yanny[2], B. Zhang[67,60], Y. Zhang[2]

(DES Collaboration)

[1] Cerro Tololo Inter-American Observatory, National Optical Astronomy Observatory, Casilla 603, La Serena, Chile
[2] Fermi National Accelerator Laboratory, P. O. Box 500, Batavia, IL 60510, USA
[3] School of Mathematics and Physics, University of Queensland, Brisbane, QLD 4072, Australia
[4] University of Copenhagen, Dark Cosmology Centre, Juliane Maries Vej 30, 2100 Copenhagen O
[5] School of Physics and Astronomy, University of Southampton, Southampton, SO17 1BJ, UK
[6] Korea Astronomy and Space Science Institute, Yuseong-gu, Daejeon, 305-348, Korea
[7] Harvard-Smithsonian Center for Astrophysics, 60 Garden St., Cambridge, MA 02138, USA
[8] Institute of Cosmology and Gravitation, University of Portsmouth, Portsmouth, PO1 3FX, UK
[9] African Institute for Mathematical Sciences, 6 Melrose Road, Muizenberg, 7945, South Africa
[10] South African Astronomical Observatory, P.O.Box 9, Observatory 7935, South Africa
[11] LSST, 933 North Cherry Avenue, Tucson, AZ 85721, USA
[12] Department of Physics and Astronomy, University of Pennsylvania, Philadelphia, PA 19104, USA
[13] CNRS, UMR 7095, Institut d'Astrophysique de Paris, F-75014, Paris, France
[14] Sorbonne Universités, UPMC Univ Paris 06, UMR 7095, Institut d'Astrophysique de Paris, F-75014, Paris, France
[15] Department of Physics & Astronomy, University College London, Gower Street, London, WC1E 6BT, UK
[16] George P. and Cynthia Woods Mitchell Institute for Fundamental Physics and Astronomy, and Department of Physics and Astronomy, Texas A&M University, College Station, TX 77843, USA
[17] Kavli Institute for Particle Astrophysics & Cosmology, P. O. Box 2450, Stanford University, Stanford, CA 94305, USA
[18] SLAC National Accelerator Laboratory, Menlo Park, CA 94025, USA
[19] Centro de Investigaciones Energéticas, Medioambientales y Tecnológicas (CIEMAT), Madrid, Spain
[20] Laboratório Interinstitucional de e-Astronomia - LIneA, Rua Gal. José Cristino 77, Rio de Janeiro, RJ - 20921-400, Brazil
[21] INAF, Astrophysical Observatory of Turin, I-10025 Pino Torinese, Italy
[22] Department of Astronomy, University of Illinois at Urbana-Champaign, 1002 W. Green Street, Urbana, IL 61801, USA
[23] National Center for Supercomputing Applications, 1205 West Clark St., Urbana, IL 61801, USA
[24] Institut de Física d'Altes Energies (IFAE), The Barcelona Institute of Science and Technology, Campus UAB, 08193 Bellaterra (Barcelona) Spain
[25] Institut d'Estudis Espacials de Catalunya (IEEC), 08034 Barcelona, Spain
[26] Institute of Space Sciences (ICE, CSIC), Campus UAB, Carrer de Can Magrans, s/n, 08193 Barcelona, Spain
[27] Physics Department, 2320 Chamberlin Hall, University of Wisconsin-Madison, 1150 University Avenue Madison, WI 53706-1390
[28] Millennium Institute of Astrophysics and Department of Physics and Astronomy, Universidad Católica de Chile, Santiago, Chile
[29] Observatório Nacional, Rua Gal. José Cristino 77, Rio de Janeiro, RJ - 20921-400, Brazil
[30] Department of Physics, IIT Hyderabad, Kandi, Telangana 502285, India
[31] Kavli Institute for Cosmological Physics, University of Chicago, Chicago, IL 60637, USA
[32] Department of Astronomy/Steward Observatory, 933 North Cherry Avenue, Tucson, AZ 85721-0065, USA
[33] Jet Propulsion Laboratory, California Institute of Technology, 4800 Oak Grove Dr., Pasadena, CA 91109, USA
[34] Department of Astronomy, University of Michigan, Ann Arbor, MI 48109, USA
[35] Department of Physics, University of Michigan, Ann Arbor, MI 48109, USA
[36] Department of Astronomy, University of California, Berkeley, CA 94720-3411, USA
[37] Miller Senior Fellow, Miller Institute for Basic Research in Science, University of California, Berkeley, CA 94720, USA
[38] Santa Cruz Institute for Particle Physics, Santa Cruz, CA 95064, USA
[39] PITT PACC, Department of Physics and Astronomy, University of Pittsburgh, Pittsburgh, PA 15260, USA
[40] Instituto de Fisica Teorica UAM/CSIC, Universidad Autonoma de Madrid, 28049 Madrid, Spain
[41] Institute of Astronomy, University of Cambridge, Madingley Road, Cambridge CB3 0HA, UK
[42] Kavli Institute for Cosmology, University of Cambridge, Madingley Road, Cambridge CB3 0HA, UK

[43] Universitäts-Sternwarte, Fakultät für Physik, Ludwig-Maximilians Universität München, Scheinerstr. 1, 81679 München, Germany

[44] Centre for Astrophysics & Supercomputing, Swinburne University of Technology, Victoria 3122, Australia

[45] California Institute of Technology, 1200 East California Blvd, MC 249-17, Pasadena, CA 91125, USA

[46] CENTRA, Instituto Superior Técnico, Universidade de Lisboa, Av. Rovisco Pais 1, 1049-001 Lisboa, Portugal

[47] Lawrence Berkeley National Laboratory, 1 Cyclotron Road, Berkeley, CA 94720, USA

[48] Department of Physics, ETH Zurich, Wolfgang-Pauli-Strasse 16, CH-8093 Zurich, Switzerland

[49] Center for Cosmology and Astro-Particle Physics, The Ohio State University, Columbus, OH 43210, USA

[50] Department of Physics, The Ohio State University, Columbus, OH 43210, USA

[51] Max Planck Institute for Extraterrestrial Physics, Giessenbachstrasse, 85748 Garching, Germany

[52] Harvard-Smithsonian Center for Astrophysics, Cambridge, MA 02138, USA

[53] Department of Physics, University of Namibia, 340 Mandume Ndemufayo Avenue, Pionierspark, Windhoek, Namibia

[54] Department of Astronomy and Astrophysics, University of Chicago, Chicago, IL 60637, USA

[55] Harvard-Smithsonian Center for Astrophysics, 60 Garden St., Cambridge, MA 02138,USA

[56] Gordon and Betty Moore Foundation, 1661 Page Mill Road, Palo Alto, CA 94304,USA

[57] Argonne National Laboratory, 9700 South Cass Avenue, Lemont, IL 60439, USA

[58] Australian Astronomical Optics, Macquarie University, North Ryde, NSW 2113, Australia

[59] Sydney Institute for Astronomy, School of Physics, A28, The University of Sydney, NSW 2006, Australia

[60] The Research School of Astronomy and Astrophysics, Australian National University, ACT 2601, Australia

[61] Departamento de Física Matemática, Instituto de Física, Universidade de São Paulo, CP 66318, São Paulo, SP, 05314-970, Brazil

[62] Institute of Astronomy and Kavli Institute for Cosmology, Madingley Road, Cambridge, CB3 0HA, UK

[63] Department of Astronomy, The Ohio State University, Columbus, OH 43210, USA

[64] Institució Catalana de Recerca i Estudis Avançats, E-08010 Barcelona, Spain

[65] Excellence Cluster Universe, Boltzmannstr. 2, 85748 Garching, Germany

[66] Faculty of Physics, Ludwig-Maximilians-Universität, Scheinerstr. 1, 81679 Munich, Germany

[67] ARC Centre of Excellence for All-sky Astrophysics (CAASTRO)

[68] Division of Theoretical Astronomy, National Astronomical Observatory of Japan, 2-21-1 Osawa, Mitaka, Tokyo 181-8588, Japan

[69] Institute of Astronomy and Astrophysics, Academia Sinica, Taipei 10617, Taiwan

[70] Department of Physics and Astronomy, Pevensey Building, University of Sussex, Brighton, BN1 9QH, UK

[71] Department of Physics, University of Arizona, Tucson, AZ 85721, USA

[72] Brandeis University, Physics Department, 415 South Street, Waltham MA 02453

[73] Instituto de Física Gleb Wataghin, Universidade Estadual de Campinas, 13083-859, Campinas, SP, Brazil

[74] Computer Science and Mathematics Division, Oak Ridge National Laboratory, Oak Ridge, TN 37831

[75] Observatories of the Carnegie Institution for Science, 813 Santa Barbara St., Pasadena, CA 91101, USA

[76] Graduate School of Education, Stanford University, 160, 450 Serra Mall, Stanford, CA 94305, USA

Draft version January 25, 2019

ABSTRACT

We present the first cosmological parameter constraints using measurements of type Ia supernovae (SNe Ia) from the Dark Energy Survey Supernova Program (DES-SN). The analysis uses a subsample of 207 spectroscopically confirmed SNe Ia from the first three years of DES-SN, combined with a low-redshift sample of 122 SNe from the literature. Our "DES-SN3YR" result from these 329 SNe Ia is based on a series of companion analyses and improvements covering SN Ia discovery, spectroscopic selection, photometry, calibration, distance bias corrections, and evaluation of systematic uncertainties. For a flat ΛCDM model we find a matter density $\Omega_{\rm m} = 0.331 \pm 0.038$. For a flat wCDM model, and combining our SN Ia constraints with those from the cosmic microwave background (CMB), we find a dark energy equation of state $w = -0.978 \pm 0.059$, and $\Omega_{\rm m} = 0.321 \pm 0.018$. For a flat $w_0 w_a$CDM model, and combining probes from SN Ia, CMB and baryon acoustic oscillations, we find $w_0 = -0.885 \pm 0.114$ and $w_a = -0.387 \pm 0.430$. These results are in agreement with a cosmological constant and with previous constraints using SNe Ia (Pantheon, JLA).

Subject headings: cosmology: supernovae

1. INTRODUCTION

Type Ia supernovae (SNe Ia) were used to discover the accelerating expansion of the universe (Riess et al. 1998, Perlmutter et al. 1999) and remain one of the key probes for understanding the nature of the mysterious 'dark energy'. Over the last two decades, there have been considerable improvements in the calibration and size of samples at low redshift (Jha et al. 2006; Hicken et al. 2009a, 2012a; Contreras et al. 2010), intermediate redshift (Holtzman et al. 2008), and high redshift (Astier et al. 2006; Wood-Vasey et al. 2007; Conley et al. 2011; Rest et al. 2014; Betoule et al. 2014). When combined with cosmic microwave background (CMB) data, these samples have been used to demonstrate that the dark energy equation of state, w, is consistent with a cosmological constant ($w = -1$) with a precision of $\sigma_w = 0.04$. The recent Pantheon analysis combines > 1000 SNe Ia from several surveys, resulting in $w = -1.026 \pm 0.041$

(Scolnic et al. 2018).

The Dark Energy Survey SN program (DES-SN) is striving to find even greater numbers of SNe while reducing systematic uncertainties on the resulting cosmological parameters. A top priority of this effort has been to accurately model each component of the DES-SN search and analysis, and to accurately simulate bias corrections for the SN Ia distance measurements. DES has also made improvements in instrumentation and calibration, including: (i) detectors with higher z-band efficiency to improve measurements of rest frame SN colors at high-redshift, and (ii) extension of the photometric calibration precision over a wide color range by correcting each CCD and exposure for atmospheric variations and the spectral energy distribution (SED) of the source (see Sect. 3). These improvements enable DES-SN to make a state-of-the-art measurement of dark energy properties.

This paper reports "DES-SN3YR" cosmological con-

straints from the spectroscopically confirmed SNe Ia in the first three years of DES-SN in combination with a low-redshift SN Ia sample from the literature. The results presented here are the culmination of a series of companion papers, which contain details of the SN search and discovery (Kessler et al. 2015; Morganson et al. 2018; Goldstein et al. 2015); spectroscopic follow-up (D'Andrea et al. 2018); photometry (Brout et al. 2018a); calibration (Burke et al. 2018; Lasker et al. 2018); simulations (Kessler et al. 2018); and technique to account for selection bias (Kessler & Scolnic 2017). The cosmological analysis method and validation are detailed in Brout et al. (2018b, B18), which presents the full statistical and systematic uncertainty budget for these new results. Hinton et al. (2018) test a new Bayesian Hierarchical Model for supernova cosmology. In this letter, we summarize these contributions and present our measurements of the equation-of-state (w) and matter density ($\Omega_{\rm m}$). Data products used in this analysis are publicly available online.[1] In addition, Macaulay et al. (2018) measure the Hubble constant (H_0) by applying these DES-SN3YR results to the inverse-distance-ladder method anchored to the standard ruler measured by baryon acoustic oscillations (Alam et al. 2017; Carter et al. 2018, BAO), and related to the sound horizon measured with CMB data (Planck Collaboration et al. 2016).

In §2 we discuss the datasets used in our analysis. In §3, we summarize the analysis pipeline. In §4, we present the cosmology results. In §5, we present our discussion and conclusions.

2. DATA SAMPLES

The DES-SN sample for this analysis was collected over three 5-month-long seasons, from August 2013 to February 2016, using the Dark Energy Camera (DECam, Flaugher et al. 2015) at the Cerro Tololo Inter-American Observatory. Ten 2.7 deg^2 fields were observed approximately once per week in the $griz$ filter bands (Abbott et al. 2018). The average depth per visit was 23.5 mag in the eight "shallow" fields, and 24.5 mag in the two "deep" fields. Within 24 hours of each observation, search images were processed (Morganson et al. 2018), new transients were discovered using a difference-imaging pipeline (Kessler et al. 2015), and most of the subtraction artifacts were rejected with a machine-learning algorithm applied to image stamps (Goldstein et al. 2015).

A subset of lightcurves was selected for spectroscopic follow-up observations (D'Andrea et al. 2018), resulting in 251 spectroscopically confirmed SNe Ia with redshifts $0.02 < z < 0.85$, and 207 SNe Ia that satisfy analysis requirements (B18) such as signal-to-noise and light curve sampling; this sample is called the DES-SN subset. The spectroscopic program required a collaborative effort coordinated across several observatories. At low to intermediate redshifts, the primary follow-up instrument is the 4-meter Anglo-Australian Telescope (AAT), which confirmed and measured redshifts for 31% of our SN Ia sample (OzDES collaboration; Yuan et al. 2015; Childress et al. 2017; Hinton et al. 2016). A variety of spectroscopic programs (D'Andrea et al. 2018) were carried out using the European Southern Observatory Very Large Telescope, Gemini, Gran Telescopio Ca-

narias, Keck, Magellan, MMT, and South African Large Telescope.

We supplement the DES-SN sample with a low-redshift ($z < 0.1$) sample, which we call the low-z subset, comprising 122 SNe from the Harvard-Smithsonian Center for Astrophysics surveys (CfA3, CfA4; Hicken et al. 2009b, 2012b) and the Carnegie Supernova Project (CSP; Contreras et al. 2010; Stritzinger et al. 2011). We only use samples with measured telescope+filter transmissions, and thus CfA1 and CfA2 are not included.

3. ANALYSIS

Supernova cosmology relies on measuring the luminosity distance (d_L) versus redshift for many SNe Ia and comparing this relation to the prediction of cosmological models. The distance modulus (μ) is defined as,

$$\mu = 5\log[d_L/10{\rm pc}]. \qquad (1)$$

For a flat universe with cold dark matter density $\Omega_{\rm m}$, dark energy density Ω_Λ, and speed of light c, the luminosity distance to a source at redshift z is given by

$$d_L = (1+z)c\int_0^z \frac{dz'}{H(z')}, \qquad (2)$$

with

$$H(z) = H_0\left[\Omega_{\rm m}(1+z)^3 + \Omega_\Lambda(1+z)^{3(1+w)}\right]^{1/2}. \qquad (3)$$

Observationally, the distance modulus of a supernova is given by

$$\mu = m_B + \alpha x_1 - \beta\mathcal{C} + M_0 + \gamma G_{\rm host} + \Delta\mu_{\rm bias}. \qquad (4)$$

For each SN Ia, the set of $griz$ light curves are fit (§3.4) to determine an amplitude (x_0, with $m_B \equiv -2.5\log(x_0)$), light curve width (x_1), and color ($\mathcal{C}$). γ describes the dependence on host-galaxy stellar mass ($M_{\rm host}$, §3.5), where $G_{\rm host} = +1/2$ if $M_{\rm host} > 10^{10}M_\odot$, and $G_{\rm host} = -1/2$ if $M_{\rm host} < 10^{10}M_\odot$. A correction for selection biases ($\Delta\mu_{\rm bias}$) is determined from simulations (§3.6).

All SNe Ia are assumed to be characterized by α, β, γ, and M_0. The first three parameters describe how the SN Ia luminiosity is correlated with the light curve width (αx_1), color ($\beta\mathcal{C}$), and host-galaxy stellar mass ($\gamma G_{\rm host}$). M_0 accounts for both the absolute magnitude of SNe Ia and the Hubble constant. In the rest of this section we describe the main components of the analysis pipeline that are needed to determine the distances (Eq. 4) and cosmological parameters.

3.1. Calibration

The DES sample is calibrated to the AB magnitude system (Oke & Gunn 1983) using measurements of the Hubble Space Telescope (HST) CalSpec standard C26202 (Bohlin et al. 2014). DES internally calibrated roughly 50 standard stars per CCD using a 'Forward Global Calibration Method' (Burke et al. 2018; Lasker et al. 2018). Improvements in calibration at the 0.01 mag (1%) level are made using SED-dependent 'chromatic corrections' to both the standard stars and to the DES-SN lightcurve photometry. The low-z sample is calibrated to the AB system by cross-calibrating to the Pan-STARRS1 (PS1) photometric catalogs (Scolnic et al. 2015). We also cross-calibrate DES to PS1 and find good agreement (see §3.1.2, Fig 3 of B18).

3.2. *Photometry*

To measure the SN Ia flux for each observation, we employ a scene modeling photometry (SMP) approach (Brout et al. 2018a) based on previous efforts used in SDSS-II (Holtzman et al. 2008) and SNLS (Astier et al. 2013). SMP simultaneously forward models a variable SN flux on top of a temporally constant host galaxy. We test the precision by analyzing images that include artificial SNe Ia, and find that photometric biases are limited to $< 0.3\%$. Each CCD exposure is calibrated to the native photometric system of DECam, and zero points are determined from the standard star catalogs (§3.1).

3.3. *Spectroscopy: Typing & Redshifts*

Spectral classification was performed using both the SuperNova IDentification (Blondin & Tonry 2007, SNID) and Superfit (Howell et al. 2005) software, as described in D'Andrea et al. (2018). All 207 events are spectroscopically classified as SNe Ia. Redshifts are obtained from host-galaxy spectra, where available, because their sharp spectral lines give more accurate redshifts ($\sigma_z \sim 5 \times 10^{-4}$; Yuan et al. 2015) than the broad SN Ia spectroscopic features ($\sigma_z \sim 5 \times 10^{-3}$). 158 of the DES-SN events have host galaxy redshifts, and the rest have redshifts from the SN Ia spectra. For the low-z sample, we use the published redshifts with a 250 km/s uncertainty from Scolnic et al. (2018). Peculiar-velocity corrections are computed from Carrick et al. (2015).

3.4. *Light-curve fitting*

To measure the SN parameters ($m_B, x_1, \mathcal{C}$), the light curves were fit with SNANA[2] (Kessler et al. 2009) using the SALT2 model (Guy et al. 2010) and the training parameters from Betoule et al. (2014).

3.5. *Host Galaxy Stellar Masses*

For the γG_{host} term in Eq. 4, we first identify the host galaxy using catalogs from Science Verification DECam images (Bonnett et al. 2016), and the directional light radius method (Sullivan et al. 2006; Gupta et al. 2016). M_{host} is derived from fitting galaxy model SEDs to $griz$ broadband fluxes with ZPEG (Le Borgne & Rocca-Volmerange 2002). The SEDs are generated with Projet d'Etude des GAlaxies par Synthese Evolutive (PEGASE: Fioc & Rocca-Volmerange 1997). In the DES-SN subset, 116 out of 207 hosts have $M_{\mathrm{host}} < 10^{10} M_\odot$. The low-$z$ host galaxy stellar masses are taken from Scolnic et al. (2018).

3.6. *μ-Bias Corrections*

We use a simulation based method (Kessler et al. 2018) to correct for distance biases arising from survey and spectroscopic selection efficiencies, and also from the analysis and light curve fitting. For each SN Ia we calculate the bias correction in Eq. 4, $\Delta\mu_{\mathrm{bias}} \equiv \langle \mu - \mu_{\mathrm{true}} \rangle$, where $\langle \rangle$ is the average in bins of measured redshift, color and stretch. The distance μ is determined by analyzing the simulated data in the same way as the real data (but with $\Delta\mu_{\mathrm{bias}} = 0$), and μ_{true} is the true distance modulus

[2] https://snana.uchicago.edu

used to generate each simulated event. The correction increases with redshift, and for individual SNe Ia can be as large as 0.4 mag (§9 of Kessler et al. 2018).

The simulation accurately models DES-SN3YR selection effects. For each generated event it picks a random redshift, color and stretch from known distributions (Perrett et al. 2012; Scolnic & Kessler 2016). Next, it computes true SN Ia magnitudes at all epochs using the SALT2 SED model, intrinsic scatter model (§3.7), telescope+atmosphere transmission functions for each filter band, and cosmological effects such as dimming, redshifting, gravitational lensing, and galactic extinction. Using the survey cadence and observing conditions (point spread function, sky noise, zero point), instrumental noise is added. Finally, our simulation models the efficiencies of DiffImg and spectroscopic confirmation. The quality of the simulation is illustrated by the good agreement between the predicted and observed distribution of many observables including redshift, stretch, and color (Figs 6 & 7 in Kessler et al. 2018, and Fig. 5 in B18).

3.7. *Intrinsic scatter model*

We simulate bias corrections with two different models of intrinsic scatter that span the range of possibilities in current data samples. First is the 'G10' model, based on Guy et al. (2010), in which the scatter is primarily achromatic. Second is the 'C11' model, based on Chotard et al. (2011), which has stronger scatter in color. For use in simulations, Kessler et al. (2013) converted each of these broadband scatter models into an SED-variation model.

3.8. *Generating the Bias-Corrected Hubble Diagram*

We use the "BEAMS with Bias Corrections" (BBC) method (Kessler & Scolnic 2017) to fit for $\{\alpha, \beta, \gamma, M_0\}$ and to fit for a weighted-average bias-corrected μ in 18 redshift bins. In addition to propagating the uncertainty from each term in Eq. 4, the BBC fit adds an empirically determined μ-uncertainty (σ_{int}) to each event so that the best fit $\chi^2/N_{\mathrm{dof}} = 1$. This redshift-binned Hubble diagram is used for cosmology fitting as described in §3.9. Fig. 1 shows the binned Hubble diagram, and also the unbinned Hubble diagram using individual bias-corrected distances computed in the BBC fit.

3.9. *Cosmology Fitting*

Cosmological parameters are constrained using the log-likelihood

$$\chi^2 = \vec{D}^T \, [C_{\mathrm{stat+syst}}]^{-1} \, \vec{D} \qquad (5)$$

and minimizing the posterior with CosmoMC (Lewis & Bridle 2002). $D_i = \mu(z_i)_{\mathrm{data}} - \mu(z_i)_{\mathrm{model}}$ for redshift bin $i = 1, 18$, $\mu(z_i)_{\mathrm{data}}$ is the BBC-fitted distance modulus in the i'th redshift bin, and $\mu(z_i)_{\mathrm{model}}$ is given by Eq. 1. The covariance matrix ($C_{\mathrm{stat+syst}}$) is described in §3.8.2 of B18, and incorporates systematic uncertainties from each analysis component in §3.

$\vec{D}$ and $C_{\mathrm{stat+syst}}$ are computed separately using the G10 and C11 scatter model in the bias-correction simulation. Each set of quantities is averaged over the G10 and C11 models, and these averages are used in Eq. 5. The purpose of averaging is to mitigate the systematic uncertainty related to our understanding of intrinsic scatter (§4.2 of B18).
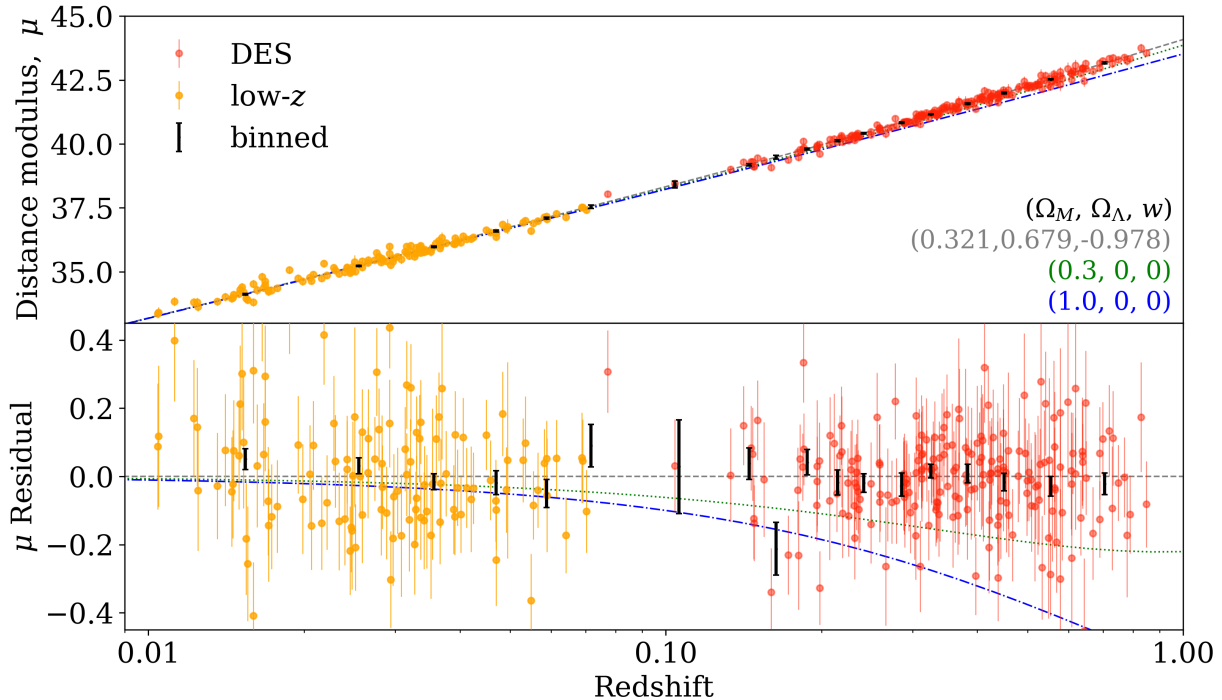
FIG. 1.— Hubble diagram for the DES-SN3YR sample. Top: Distance modulus (μ) from BBC fit (black bars, which are used for cosmology fits) and for each SN (red, orange circles). The dashed gray line shows our best fit model, while the green and blue dotted lines show models with no dark energy and matter densities $\Omega_m = 0.3$ and 1.0 respectively. Bottom: Residuals to the best fit model; 1σ error bars show 68% confidence.

Finally, we combine these SN Ia results with priors from CMB and BAO as described in §4.

3.10. Blinding and Validation

The cosmological parameters were blinded until preliminary results were presented at the 231st meeting of the American Astronomical Society in January 2018. The criteria for unblinding (§7 of B18) included analyzing large simulated DES-SN3YR data sets, and requiring i) w-bias below 0.01, and ii) the rms of w-values agrees with the fitted w-uncertainty, for simulations with and without systematic variations. Following this initial unblinding, several updates were performed (§3.8.4 of B18), again blinded, and the final results presented here were unblinded during the DES internal review process. Compared to the initial unblinding, w increased by 0.024 and the total uncertainty increased by 3% (0.057 to 0.059).

4. RESULTS

We present the first cosmological results using SNe Ia from DES. We begin with the BBC-fitted parameters ($\alpha, \beta, \gamma, \sigma_{\rm int}$) in §4.1, then present our statistical and systematic uncertainty budget for w in §4.2 and Table 1. Finally, we present our cosmological parameters in §4.3 and Table 2. For our primary results we combine DES-SN3YR with the CMB likelihood from Planck Collaboration et al. 2016 using their temperature power spectrum and low-ℓ polarization results. We also present results without a CMB prior, and with both CMB and BAO priors. All reported uncertainties correspond to 68% confidence. To evaluate consistency between our primary re-
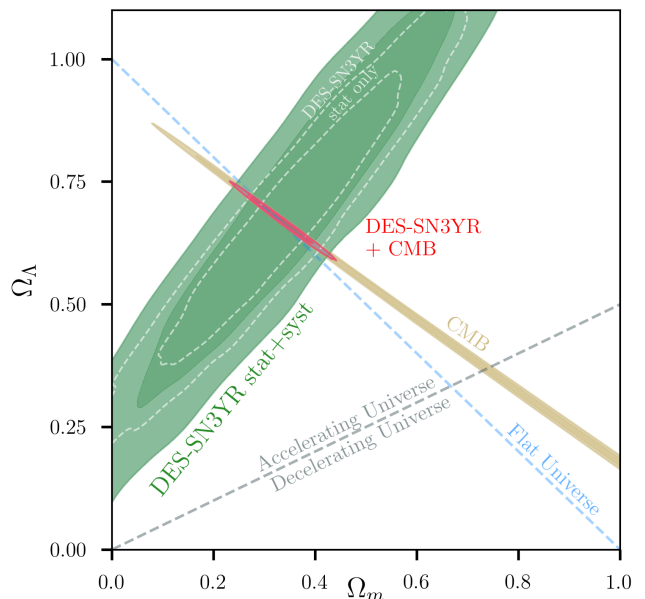
FIG. 2.— Constraints on Ω_m-Ω_Λ for ΛCDM model (68% and 95% confidence intervals). SN contours are shown with statistical uncertainty only (white-dashed), and with total uncertainty (green shaded). Constraints from CMB (brown) and DES-SN3YR+CMB combined (red), are also shown.

sult and BAO, we compute the evidence using `PolyChord` (Handley et al. 2015a,b), and compute the evidence ratio (R) defined in Eq. V.3 of DES Collaboration et al.

(2017). Consistency is defined by $R > 0.1$.

4.1. *Results for Standardization Parameters*

While the cosmology results are based on averaging distances using the G10 and C11 intrinsic scatter models, here we show best-fit BBC values from B18 using the G10 intrinsic scatter model: $\alpha = 0.146 \pm 0.009$, $\beta = 3.03 \pm 0.11$, $\gamma = 0.025 \pm 0.018$, and $\sigma_{\rm int} = 0.094 \pm 0.008$. Our α, β, and $\sigma_{\rm int}$ values are consistent with those found in previous analyses, while γ is smaller compared to those in Kelly et al. (2010); Sullivan et al. (2010); Lampeitl et al. (2010); Betoule et al. (2014); Scolnic et al. (2018). Results with the C11 model (Table 5 of B18) show similar trends.

We also check the consistency among the DES-SN and low-z subsets. While α and β are consistent, we find $\sigma_{\rm int} = 0.066 \pm 0.006$ for DES-SN, the lowest value of any rolling SN survey. This value differs by 3.3σ from $\sigma_{\rm int} = 0.120 \pm 0.015$ for the low-z subset, and the systematic uncertainty in adopting a single $\sigma_{\rm int}$ value is discussed below in §4.2 and also in §7.3 of B18. Our γ values differ by 1.5σ: $\gamma_{\rm DES} = 0.009 \pm 0.018$ (consistent with zero) and $\gamma_{{\rm low}z} = 0.070 \pm 0.038$.

4.2. *w Uncertainty Budget*

Contributions to the systematic uncertainty budget are presented in B18 and shown here in Table 1 for flat wCDM fits combined with the CMB likelihood. The statistical uncertainty on w ($\sigma_{w,{\rm stat}}$) is determined without systematic contributions. Each systematic contribution is defined as

$$\sigma_{w,{\rm syst}} = \sqrt{(\sigma_{w,{\rm tot}})^2 - (\sigma_{w,{\rm stat}})^2} \qquad (6)$$

where $\sigma_{w,{\rm tot}}$ is the total (stat+syst) uncertainty from including a specific systematic, or a group of systematics. The uncertainty in w has nearly equal contributions from statistical and systematic uncertainties, the latter of which is broken into four groups in Table 1.

The first three systematic groups have nearly equal contributions: 1) photometry and calibration ($\sigma_w = 0.021$), which includes uncertainties from the DES-SN and low-z subsets, data used to train the SALT2 lightcurve model, and the HST Calspec standard, 2) μ-bias corrections from the survey ($\sigma_w = 0.023$), which includes uncertainties from rejecting Hubble residual outliers in the low-z subset, magnitude versus volume limited selection for low-z, DES-SN spectroscopic selection efficiency, and determination of DES-SN flux uncertainties, and 3) μ-bias corrections from astrophysical effects ($\sigma_w = 0.026$), which includes uncertainties from intrinsic scatter modeling (G10 vs. C11, and two $\sigma_{\rm int}$, parent populations of stretch and color, choice of w and $\Omega_{\rm m}$ in the simulation, and Galactic extinction. The 4th systematics group, redshift ($\sigma_w = 0.012$), includes a global shift in the redshift and peculiar velocity corrections.

Finally, the Table 1 systematics marked with a dagger (†) have not been included in previous analyses, and the combined uncertainty is $\sigma_w = 0.024$. Most of this new uncertainty is related to the low-z subset, which is almost 40% of the DES-SN3YR sample. For previous analyses with a smaller fraction of low-z events (e.g., Pantheon, JLA) we do not recommend adding the full 0.024 w-uncertainty to their results.

TABLE 1
w UNCERTAINTY CONTRIBUTIONS FOR wCDM MODEL[a]

Description[b]	σ_w	$\sigma_w/\sigma_{w,{\rm stat}}$
Total Stat ($\sigma_{w,{\rm stat}}$)	0.042	1.00
Total Syst[c]	0.042	1.00
Total Stat+Syst	0.059	1.40
[Photometry & Calibration]	**[0.021]**	**[0.50]**
Low-z	0.014	0.33
DES	0.010	0.24
SALT2 model	0.009	0.21
HST Calspec	0.007	0.17
[μ-Bias Correction: survey]	**[0.023]**	**[0.55]**
†Low-z 3σ Cut	0.016	0.38
Low-z Volume Limited	0.010	0.24
Spectroscopic Efficiency	0.007	0.17
†Flux Err Modeling	0.001	0.02
[μ-Bias Correction: astrophysical]	**[0.026]**	**[0.62]**
Intrinsic Scatter Model (G10 vs. C11)	0.014	0.33
†Two $\sigma_{\rm int}$	0.014	0.33
$\mathcal{C}$, x_1 Parent Population	0.014	0.33
†w, $\Omega_{\rm m}$ in sim.	0.006	0.14
MW Extinction	0.005	0.12
[Redshift]	**[0.012]**	**[0.29]**
Peculiar Velocity	0.007	0.17
†$z + 0.00004$	0.006	0.14

[a] The sample is DES-SN3YR (DES-SN + low-z sample) plus CMB prior.
[b] Item in [**bold**] is a sub-group and its uncertainty.
[c] The quadrature sum of all systematic uncertainties does not equal 0.042 because of redshift-dependent correlations when using the full covariance matrix.
† Uncertainty was not included in previous analyses.

4.3. *Cosmology results*

4.3.1. Λ*CDM*

Using DES-SN3YR and assuming a flat ΛCDM model, we find $\Omega_{\rm m} = 0.331 \pm 0.038$. Assuming a ΛCDM model with curvature ($\Omega_{\rm k}$) added as a free parameter in Eq. 3 (e.g., see Sect 3.1 of Davis & Parkinson 2017) we find the constraints shown in Fig. 2 and Table 2 (row 2). Solid contours show our result with both statistical and systematic uncertainties included, while dashed contours show the statistical-only uncertainties for comparison. Fig. 2 also shows that the CMB data provide strong flatness constraints, consistent with zero curvature; the impact of using this CMB prior is shown in row 3. The impact from adding a BAO prior is shown in row 4, where the evidence ratio $R = 110$ shows consistency between the SN+CMB and BAO posteriors.

4.3.2. *Flat w*CDM

For our primary result, we use DES-SN3YR with the CMB prior and a flat wCDM model ($\Omega_{\rm k} = 0$) and find $\Omega_{\rm m} = 0.321 \pm 0.018$ and $w = -0.978 \pm 0.059$ (Table 2, row 5). Our constraint on w is consistent with the cosmological-constant model for dark energy. The 68% and 95% confidence intervals are given by the red contours in Fig. 3, which also shows the contributions from DES-SN3YR and CMB. We show two contours for DES-SN3YR, with and without systematic uncertainties in order to demonstrate their impact. In Table 2, row 6, we show the impact of the low-redshift SN sample by re-
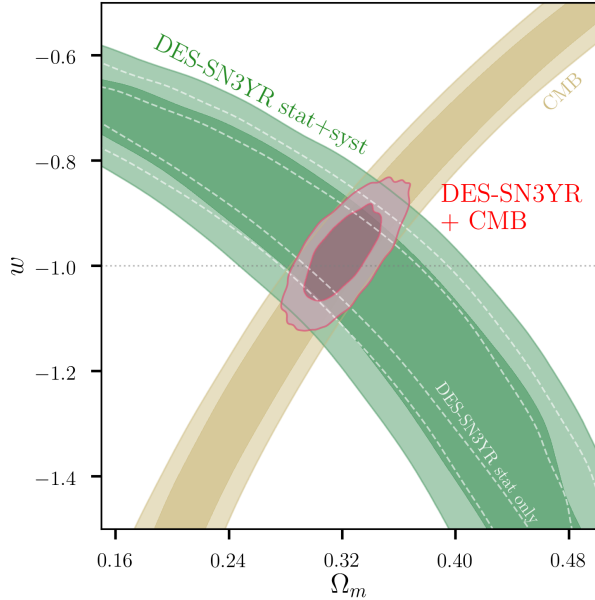
FIG. 3.— Constraints on $\Omega_{\rm m}$-w for the flat wCDM model (68% and 95% confidence intervals). SN contours are shown with only statistical uncertainty (white-dashed) and with total uncertainty (green-shaded). Constraints from CMB (brown) and DES-SN3YR+CMB combined (red) are also shown.

moving it; the w-uncertainty increases by 25% and the constraint lies approximately 1σ from $w = -1$.

Next, we consider other combinations of data. Adding a BAO prior (Alam et al. 2017; Ross et al. 2015; Beutler et al. 2011) in addition to the CMB prior and SN constraints, our best fit w-value (Table 2, row 7) is shifted by only 0.006, the uncertainty is reduced by $\sim 20\%$ compared to our primary result, and the evidence ratio between SN+CMB and BAO is $R = 81$ showing consistency among the data sets. If we remove the low-z SN subset (row 8), the w-uncertainty increases by only $\sim 8\%$. Furthermore, we remove the SN sample entirely and find that the w-uncertainty increases by nearly 50% (row 9).

4.3.3. *Flat $w_0 w_a$CDM*

Our last test is for w evolution using the $w_0 w_a$CDM model, where $w = w_0 + w_a(1 - a)$ and $a = (1 + z)^{-1}$. Combining probes from SNe, CMB, and BAO, we find results (Table 2, row 10) consistent with a cosmological constant $(w_0, w_a = -1, 0)$ and a figure of merit (Albrecht et al. 2006) of 45.5. Removing the SN sample increases the w_0 and w_a uncertainties by a factor of 2 and 1.5, respectively (row 11).

4.4. *Comparison to other SN Ia Surveys/Analyses*

The DES-SN3YR result has competitive constraining power given the sample size ($\sigma_{w,\rm tot} = 0.059$ with 329 total SNe Ia), even after taking into account additional sources of systematic uncertainty. While our DES-SN3YR sample is $< 1/3$ the size of the Pantheon sample (PS1+SNLS+SDSS+low-z+HST, $\sigma_{w,\rm tot} = 0.041$), our low-$z$ subset is 70% the size of Pantheon's low-z subset, and we included five additional sources of systematic uncertainty, our improvements (§1) result in a w-uncertainty that is only $\times 1.4$ larger.

5. DISCUSSION AND CONCLUSION

We have presented the first cosmological results from the DES-SN program: $\Omega_{\rm m} = 0.321 \pm 0.018$ and $w = -0.978 \pm 0.059$ for a flat wCDM model after combining with CMB constraints. These results are consistent with a cosmological constant model and demonstrate the high constraining power (per SN) of the DES-SN sample. DES-SN3YR data products used in this analysis are publicly available at https://des.ncsa.illinois.edu/releases/sn. These products include filter transmissions, redshifts, light curves, host masses, light-curve fit parameters, Hubble Diagram, bias corrections, covariance matrix, MC chains, and code releases.

We have utilized the spectroscopically confirmed SN Ia sample from the first three years of DES-SN as well as a low-redshift sample. This 3-year sample contains $\sim 10\%$ of the SNe Ia discovered by DES-SN over the full five year survey. Many of the techniques established in this analysis will form the basis of upcoming analyses on the much larger 5-year photometrically identified sample.

To benefit from the increased statistics in the 5-year sample it will be critical to reduce systematic uncertainties. We are working to improve calibration with a large sample of DA White Dwarf observations, including two HST Calspec standards. Other improvements to systematics are discussed in §7.2 of B18. We are optimistic that our systematic uncertainties can remain at the level of our statistical uncertainties for the 5-year analysis. This progress in understanding systematics will be critical for making new, exciting measurements of dark energy and for paving the way towards Stage-IV dark energy experiments like LSST and WFIRST.

TABLE 2
Cosmological results[a]

Row	SN Sample + Prior (ΛCDM)	Ω_m	Ω_Λ	
1	**DES-SN3YR**[b]**+flatness**	0.331 ± 0.038	0.669 ± 0.038	
2	DES-SN3YR	0.332 ± 0.122	0.671 ± 0.163	
3	DES-SN3YR+CMB[c]	0.335 ± 0.042	0.670 ± 0.032	
4	DES-SN3YR+CMB+BAO[d]	0.308 ± 0.007	0.690 ± 0.008	
	SN Sample + Prior (Flat wCDM)	Ω_m	w	
5	**DES-SN3YR+CMB**	0.321 ± 0.018	-0.978 ± 0.059	
6	DES-SN[e]+CMB	0.341 ± 0.027	-0.911 ± 0.087	
7	DES-SN3YR+CMB+BAO	0.311 ± 0.009	-0.977 ± 0.047	
8	DES-SN+CMB+BAO	0.315 ± 0.010	-0.959 ± 0.054	
9	CMB+BAO	0.310 ± 0.013	-0.988 ± 0.072	
	SN Sample + Prior (Flat $w_0 w_a$CDM)	Ω_m	w_0	w_a
10	**DES-SN3YR+CMB+BAO**	0.316 ± 0.011	-0.885 ± 0.114	-0.387 ± 0.430
11	CMB+BAO	0.332 ± 0.022	-0.714 ± 0.232	-0.714 ± 0.692

[a] Samples in bold font are primary results given in the abstract.
[b] DES-SN3YR: DES-SN + Low-z samples.
[c] CMB: Planck TT + lowP likelihood (Planck Collaboration et al. 2016).
[d] BAO: SDSS DR12 (Alam et al. 2017); SDSS MGS (Ross et al. 2015); 6dFGS (Beutler et al. 2011)
[e] DES-SN alone (no low-z).

REFERENCES

Abbott, T. M. C., Abdalla, F. B., Allam, S., et al. 2018, ArXiv e-prints, arXiv:1801.03181
Alam, S., Ata, M., Bailey, S., et al. 2017, MNRAS, 470, 2617
Albrecht, A., Bernstein, G., Cahn, R., et al. 2006, ArXiv Astrophysics e-prints, astro-ph/0609591

Astier, P., Guy, J., Regnault, N., et al. 2006, A&A, 447, 31
Astier, P., El Hage, P., Guy, J., et al. 2013, A&A, 557, A55
Betoule, M., Kessler, R., Guy, J., et al. 2014, A&A, 568, A22
Beutler, F., Blake, C., Colless, M., et al. 2011, MNRAS, 416, 3017
Blondin, S., & Tonry, J. L. 2007, ApJ, 666, 1024

Bohlin, R. C., Gordon, K. D., & Tremblay, P.-E. 2014, PASP, 126, 711

Bonnett, C., Troxel, M. A., Hartley, W., et al. 2016, Phys. Rev. D, 94, 042005

Brout, D. 2018, in American Astronomical Society Meeting Abstracts, Vol. 231, American Astronomical Society Meeting Abstracts #231, 219.04

Brout, D., Sako, M., & Scolnic, D. 2018a, arXiv:1811.02378

Brout, D., Scolnic, D., & Kessler, R. 2018b, arXiv:1811.02377

Burke, D. L., Rykoff, E. S., Allam, S., et al. 2018, AJ, 155, 41

Carrick, J., Turnbull, S. J., Lavaux, G., & Hudson, M. J. 2015, MNRAS, 450, 317

Carter, P., Beutler, F., Percival, W. J., et al. 2018, MNRAS, 481, 2371

Childress, M. J., Lidman, C., Davis, T. M., et al. 2017, MNRAS, 472, 273

Chotard, N., Gangler, E., Aldering, G., et al. 2011, A&A, 529, L4

Conley, A., Guy, J., Sullivan, M., et al. 2011, ApJS, 192, 1

Contreras, C., Hamuy, M., Phillips, M. M., et al. 2010, AJ, 139, 519

D'Andrea, C., Smith, M., & Sullivan, M. 2018, ArXiv:1811.09565, arXiv:1811.09565

Davis, T. M., & Parkinson, D. 2017, Characterizing Dark Energy Through Supernovae, ed. A. W. Alsabti & P. Murdin, 2623

DES Collaboration, Abbott, T. M. C., Abdalla, F. B., et al. 2017, ArXiv e-prints, arXiv:1708.01530

Fioc, M., & Rocca-Volmerange, B. 1997, A&A, 326, 950

Flaugher, B., Diehl, H. T., Honscheid, K., et al. 2015, AJ, 150, 150

Goldstein, D. A., D'Andrea, C. B., Fischer, J. A., et al. 2015, AJ, 150, 82

Gupta, R. R., Kuhlmann, S., Kovacs, E., et al. 2016, AJ, 152, 154

Guy, J., Sullivan, M., Conley, A., et al. 2010, A&A, 523, A7

Handley, W. J., Hobson, M. P., & Lasenby, A. N. 2015a, MNRAS, 450, L61

—. 2015b, MNRAS, 453, 4384

Hicken, M., Wood-Vasey, W. M., Blondin, S., et al. 2009a, ApJ, 700, 1097

Hicken, M., Challis, P., Jha, S., et al. 2009b, ApJ, 700, 331

Hicken, M., Challis, P., Kirshner, R. P., et al. 2012a, ApJS, 200, 12

—. 2012b, ApJS, 200, 12

Hinton, S., Kim, A., & Davis, T. 2018, arXiv:1811.02381

Hinton, S. R., Davis, T. M., Lidman, C., Glazebrook, K., & Lewis, G. F. 2016, Astronomy and Computing, 15, 61

Holtzman, J. A., Marriner, J., Kessler, R., et al. 2008, AJ, 136, 2306

Howell, D. A., Sullivan, M., Perrett, K., et al. 2005, ApJ, 634, 1190

Jha, S., Kirshner, R. P., Challis, P., et al. 2006, AJ, 131, 527

Kelly, P. L., Hicken, M., Burke, D. L., Mandel, K. S., & Kirshner, R. P. 2010, ApJ, 715, 743

Kessler, R., Brout, D., & Crawford, S. 2018, arXiv:1811.02379

Kessler, R., & Scolnic, D. 2017, ApJ, 836, 56

Kessler, R., Bernstein, J. P., Cinabro, D., et al. 2009, PASP, 121, 1028

Kessler, R., Guy, J., Marriner, J., et al. 2013, ApJ, 764, 48

Kessler, R., Marriner, J., Childress, M., et al. 2015, AJ, 150, 172

Lampeitl, H., Smith, M., Nichol, R. C., et al. 2010, ApJ, 722, 566

Lasker, J., Kessler, R., & Scolnic, D. 2018, arXiv:1811.02380

Le Borgne, D., & Rocca-Volmerange, B. 2002, A&A, 386, 446

Lewis, A., & Bridle, S. 2002, Phys. Rev., D66, 103511

Macaulay, E., Nichol, R. C., & Bacon, D. 2018, arXiv:1811.02376

Morganson, E., Gruendl, R. A., Menanteau, F., et al. 2018, PASP, 130, 074501

Oke, J. B., & Gunn, J. E. 1983, ApJ, 266, 713

Perlmutter, S., Aldering, G., Goldhaber, G., et al. 1999, ApJ, 517, 565

Perrett, K., Sullivan, M., Conley, A., et al. 2012, AJ, 144, 59

Planck Collaboration, Ade, P. A. R., Aghanim, N., et al. 2016, A&A, 594, A13

Rest, A., Scolnic, D., Foley, R. J., et al. 2014, ApJ, 795, 44

Riess, A. G., Filippenko, A. V., Challis, P., et al. 1998, AJ, 116, 1009

Ross, A. J., Samushia, L., Howlett, C., et al. 2015, MNRAS, 449, 835

Scolnic, D., & Kessler, R. 2016, ApJ, 822, L35

Scolnic, D., Casertano, S., Riess, A., et al. 2015, ApJ, 815, 117

Scolnic, D. M., Jones, D. O., Rest, A., et al. 2018, ApJ, 859, 101

Stritzinger, M. D., Phillips, M. M., Boldt, L. N., et al. 2011, AJ, 142, 156

Sullivan, M., Le Borgne, D., Pritchet, C. J., et al. 2006, ApJ, 648, 868

Sullivan, M., Conley, A., Howell, D. A., et al. 2010, MNRAS, 406, 782

Wood-Vasey, W. M., Miknaitis, G., Stubbs, C. W., et al. 2007, ApJ, 666, 694

Yuan, F., Lidman, C., Davis, T. M., et al. 2015, MNRAS, 452, 3047